



ELSEVIER

Available online at [www.sciencedirect.com](http://www.sciencedirect.com)

NDT&amp;E International ■ (■■■■) ■■■-■■■

**NDT&E**  
international[www.elsevier.com/locate/ndteint](http://www.elsevier.com/locate/ndteint)

# Directional filter bank-based segmentation for improved evaluation of nondestructive evaluation images

Gokul Swamy, Krishnan Balasubramaniam\*

*Centre for Nondestructive Evaluation and Department of Mechanical Engineering, Indian Institute of Technology Madras, Chennai 600 036, India*

Received 20 August 2005; received in revised form 15 August 2006; accepted 3 October 2006

## Abstract

This paper introduces a directional filter bank (DFB) for segmentation of NDE images containing directional information. The DFB is used to split an image into a desired number of sub-band images with each sub-band image containing features belonging only to a given angular range. The DFB is a two-channel decomposition employing the Quincunx sampling matrix and the diamond half band filter pair. The DFB is also designed to incorporate the property of perfect reconstruction or alias free reconstruction. Applications of the DFB towards segmenting C-scan images of fiber-reinforced composites, magnetic flux leakage (MFL) images of seamless tubes, IR images of solar cell panels and optical images for the computation of area coverage in a shot-peening process are discussed.

© 2006 Published by Elsevier Ltd.

*Keywords:* Filter bank; Quincunx sampling; Shot-peening; MFL images; Ultrasonic C-scan images

## 1. Introduction

Non-destructive evaluation (NDE) images have been widely used to detect and characterize defects and irregularities in structural components. NDE data that are represented in the form of images often have two important classes of information. These are (a) information about defects/anomalies that are present in the structure/component, and (b) characteristics of the materials/structure such as micro-structural features, geometrical boundaries, machining marks, etc. The relevance of either type of information is clearly application dependent. Usually, the NDE images have both information superimposed hence the interpretation and eventually the quantitative assessment of these images are detrimentally affected.

Hence, there is a need for techniques that can decouple the above information, or at least reduce the influence of one on the other. This is schematically illustrated in Fig. 1 where an ultrasonic C-scan image of a fiber-reinforced composite with both fiber as well as defects is imaged.

It would be desirable to separate the fiber information from defect features. Here, the fibers are oriented in specific directions, depending on the fiber lay-up used during manufacturing, while the defects are considered not to have orientations in these directions. For accomplishing this separation, a directional filter bank (DFB) technique is described in this paper in order to extract directional features from images.

The DFB splits the frequency spectrum into fan-shaped pass bands, which can then be used to extract directional features from the images. Fig. 2 shows the Fourier spectrum of the C-scan image depicted in Fig. 1. The streaks in the Fourier spectrum indicate the directionality of the fiber orientation. It can be shown that the streaks will lie on a line perpendicular to the actual fiber orientation [1].

Mallat [2] was the first to propose the concept of a filter bank for multi-frequency channel decomposition of images. The concept of a filter bank for directional decomposition of images was proposed by Bamberger and Smith [3]. Their paper however did not include a method for designing the analysis and synthesis filters satisfying the perfect reconstruction (PR) property. A lot of

\*Corresponding author. Tel./fax: +91 044 222578588.

E-mail address: [balas@iitm.ac.in](mailto:balas@iitm.ac.in) (K. Balasubramaniam).

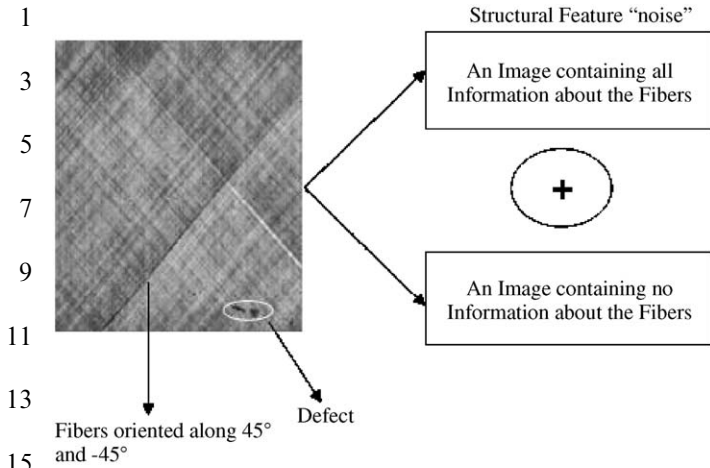


Fig. 1. Conceptual implementation of DFB-based image segmentation.

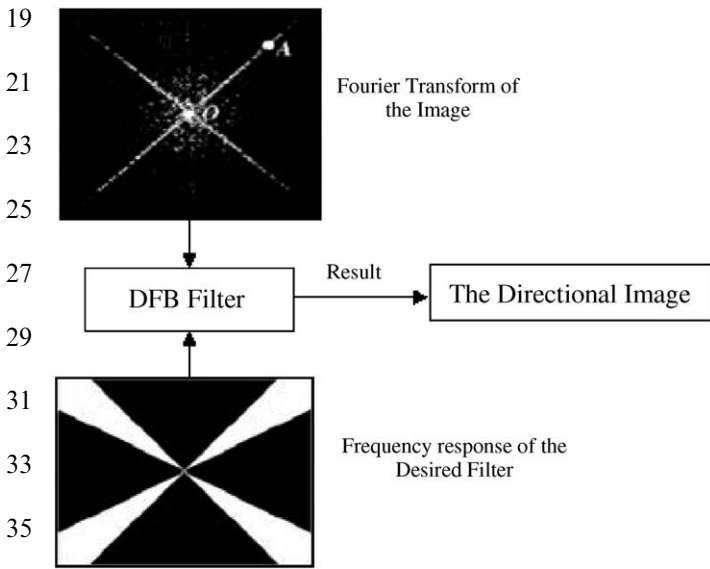


Fig. 2. Schematic of the DFB for extracting directional features.

work [4,5] has been reported in the area of developing analysis and synthesis filters to satisfy the PR property.

This paper begins by giving a description of the DFB followed by a method to design analysis and synthesis filters satisfying the PR property. Finally some results demonstrating the application of the DFB towards directional segmentation of C-scan images from fiber-reinforced composites, MFL images of seamless tubes, IR images of solar cell panels and visual photographic images of shot-peened surfaces are presented.

## 51 2. Filter bank architecture

53 The DFB decomposes the input image into a set of  $2^{n+1}$  sub-band images ( $n$  being the number of cascades) with each sub-band having a wedge-shaped frequency response. Fig. 3 shows the wedge-shaped responses for 8-band decomposition. These wedge-shaped frequency pass-bands

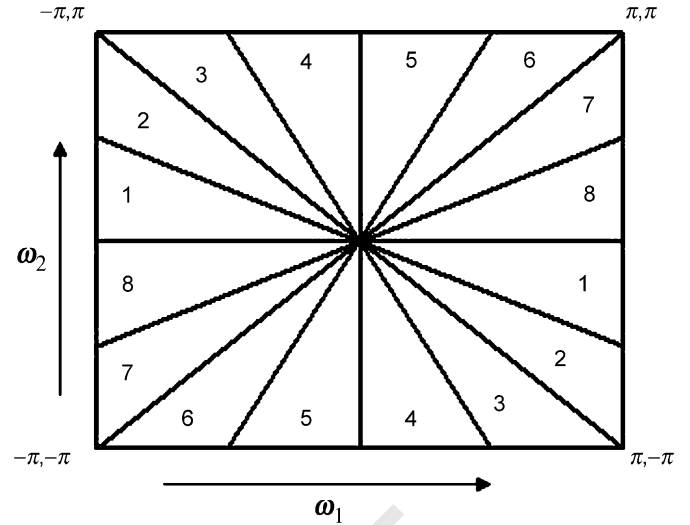


Fig. 3. Wedge-shaped frequency response for an 8-band decomposition.

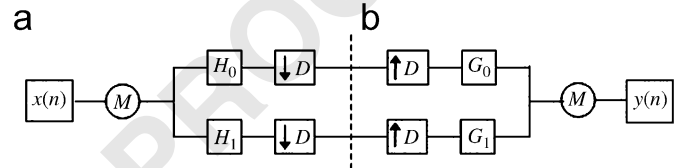


Fig. 4. (a) Analysis bank for 2-band decomposition and (b) synthesis bank.

correspond to image features having an angular orientation perpendicular to the wedge in the spatial domain.

An increase in the number of sub-bands leads to an increase in the number of wedge-shaped pass bands and a corresponding increase in the angular resolution of the directional decomposition.

Fig. 4 shows the filter bank for the two-band decomposition. Fig. 4(a) is the analysis bank and Fig. 4(b) is the interpolation or the synthesis bank.  $D$  is the Quincunx sampling matrix as given by (1).

$$D = \begin{bmatrix} 1 & -1 \\ -1 & 1 \end{bmatrix}. \quad (1)$$

A down ( $\downarrow$ ) arrow represents a downsampling operation and an up ( $\uparrow$ ) arrow represents an upsampling operation. Detailed description of the sampling operations and multirate signal-processing identities can be found in [5].  $H_0$ ,  $H_1$  and  $G_0$ ,  $G_1$  are the low pass and high pass analysis and synthesis filters, respectively.  $M$  represents modulation by  $\pi$  in the frequency variable  $\omega_1$ . The filter paths leading to the generation of the two sub-band outputs  $y_1(n)$  and  $y_2(n)$  are shown in Fig. 5. The frequency response of the two sub-band outputs for the two-band decomposition is shown in Fig. 6. A four-band output can be obtained by cascading the analysis and synthesis filters as shown in Fig. 7.

The sub-band outputs (the outputs of the individual filter paths) for eight-band decomposition have wedge-shaped frequency responses as shown in Fig. 3. Eight-band decompositions can be obtained by appropriately cascading the sub-bands of the four-band decomposition by the analysis and synthesis filter bank shown in Fig. 8. Expressions for the resampling matrix are given below

$$R_1 = \begin{bmatrix} 1 & -1 \\ 0 & 1 \end{bmatrix}, \quad R_2 = \begin{bmatrix} 1 & 1 \\ 0 & 1 \end{bmatrix},$$

$$R_3 = \begin{bmatrix} -1 & 0 \\ 0 & 1 \end{bmatrix}, \quad R_4 = \begin{bmatrix} 1 & 0 \\ 1 & 1 \end{bmatrix}. \quad (2)$$

Analysis and synthesis filters  $H_0$ ,  $H_1$ ,  $G_0$  and  $G_1$  were designed using a paraunitary formulation (refer to Appendix A for a detailed description of the design procedure). The impulse response of the filters  $H_0$ ,  $H_1$  are given in Tables 1 and 2, respectively. The filters  $G_0$  and  $G_1$  can be obtained using the relation.

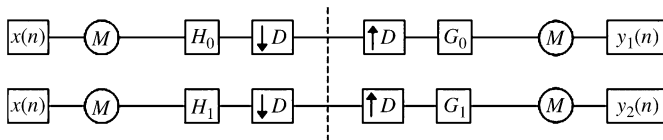


Fig. 5. Filter paths leading to the generation of the two sub-band outputs.

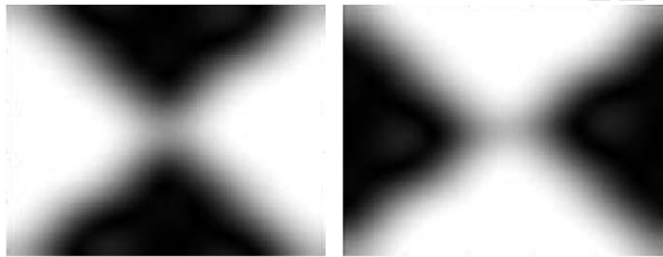


Fig. 6. Wedge-shaped frequency response of two sub-band outputs.

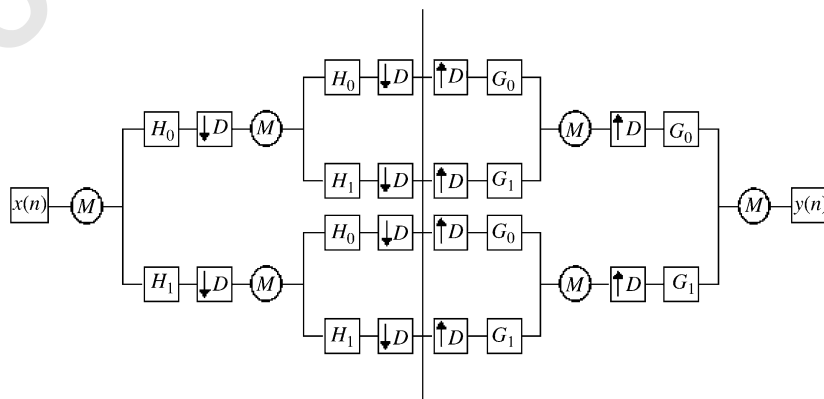


Fig. 7. DFB for 4-band decomposition.

$$G_0(i, j) = -H_1(i, j)^*(-1)^{i+j},$$

$$G_1(i, j) = -H_0(i, j)^*(-1)^{i+j}. \quad (3)$$

### 3. Results and analysis

The results of applying the DFB algorithm towards segmenting NDE images from ultrasonic, magnetic flux leakage (MFL), infrared and optical inspection are presented in this section.

#### 3.1. Segmentation of ultrasonic C-scans of composite laminates

Fiber-reinforced composite materials have gained prominence in recent times due to their high strength to weight ratio. Very often the properties of a composite material depend on the layout of its reinforced fibers. Hence it becomes very essential to determine the fiber orientation in a composite material to determine its properties [6,7]. The ultrasonic C-scan image of a fiber-reinforced composite contains a characteristic pattern oriented along the fiber direction due to backscattering of the incident ultrasonic field by the fibers.

A method for mapping fiber orientations in composite laminates using two-dimensional FFT was described by Fei et al. [8]. In many situations the presence of features related to the fibers in the C-scan image can prove to be an impediment towards automatic defect detection. In such cases it becomes necessary to be able to segment the defect information from that of the fibers prior to performing any automatic defect recognition.

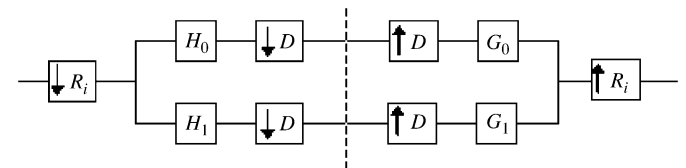


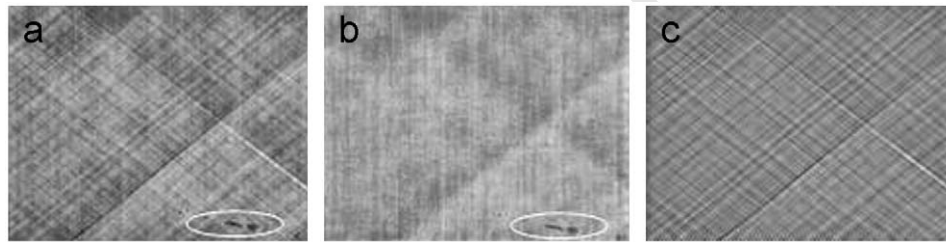
Fig. 8. Analysis and synthesis bank for cascading the 4-band decomposition.

1 Table 1  
Impulse response of filter  $H_0$

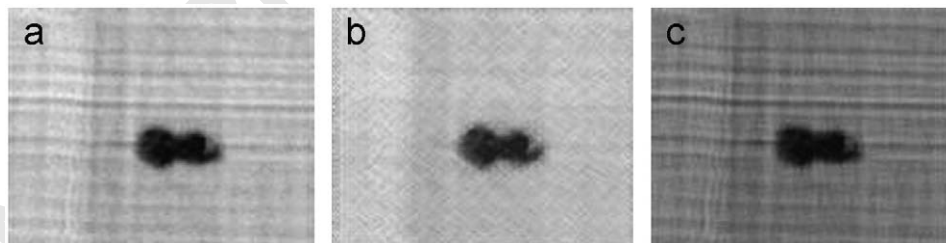
3	0	0	0	-0.0004	0	0	0	59
	0	0	0.0018	0.0009	0.0031	0	0	61
5	0	-0.0082	-0.0015	-0.0091	-0.0073	-0.0020	0	63
	-0.0017	-0.0014	0.0731	0.0002	-0.0147	0.0049	0.0386	65
7	-0.0007	0.0228	-0.0446	-0.0903	0.0495	-2.011	-0.0923	67
	-0.0064	0.0174	-0.0590	0.2751	0.7486	0.2091	0.0101	69
9	-0.0027	0.0324	-0.0646	0.1047	0.4609	0.0201	-0.0241	71
	0	0.0136	0.0373	-0.0022	0.0212	-0.1189	0	73
	0	0	0.0156	-0.0137	0.0257	0	0	75
11	0	0	0	-0.0057	0	0	0	77

13 Table 2  
Impulse response of filter  $H_1$

15	0	0	0	0.0057	0	0	0	79
17	0	0	-0.0257	-0.0137	-0.0156	0	0	81
	0	0.1189	0.0212	0.0022	0.0373	-0.0136	0	83
19	0.0241	0.0201	-0.4609	0.1047	0.0646	0.0324	0.0027	85
	0.0101	-0.2091	0.7486	-0.2751	-0.0590	-0.0174	-0.0064	87
21	0.0923	-0.2011	-0.0495	-0.0903	0.0446	0.0228	0.0007	89
	0.0386	-0.0049	-0.0147	-0.0002	0.0731	0.0014	-0.0017	91
	0	-0.0020	0.0073	-0.0091	0.0015	-0.0082	0	93
23	0	0	0.0031	-0.0009	0.0018	0	0	95
	0	0	0	-0.0004	0	0	0	97



27 Fig. 9. (a) Original C-scan image with defect circled, (b) segmented image after removing fibers and (c) segmented image containing the fibers.



29 Fig. 10. (a) C-Scan from an impacted composite, (b) segmented image after removal of fiber pattern and (c) segmented image depicting an enhanced fiber pattern.

31 Fig. 9(a) shows an ultrasonic C-scan image from a fiber-reinforced composite with fiber orientation along 45° and -45°. The region marked by the white circle is a small defect in the interior of the specimen. This image was segmented using 8-band decomposition. The sum of the images from the sub-bands 1, 4, 5 and 8 (as described in Fig. 3) is shown in Fig. 9(b). Since these sub-bands are not sensitive to the fiber direction the image contains informa-

tion pertaining mainly to the defect. The sum of the images from the sub-bands 2, 3, 6 and 7 is shown in Fig. 9(c). As can be clearly seen these sub-bands are sensitive to the fiber direction and clearly shows the fibers. The PR property implies that the sum of the images in Fig. 9(b) and (c) is exactly equal to the input image shown in Fig. 9(a).

Another ultrasonic C-scan image, shown in Fig. 10(a), was decomposed using DFB. This cross-ply graphite epoxy

laminated sample possessed a relatively large delamination defect induced due to impact. The segmented image in Fig. 10(b) shows that the fiber pattern is significantly reduced while enhancing the defect image. Since the defect was relatively large and has representation in all directions, the residue filter image in Fig. 10(c) was unable to remove the defect from the image, but it can be observed that the fiber pattern is enhanced when compared to original undecomposed C-scan image.

In order to demonstrate the improvement in the defect sizing, the images in Fig. 10(a) and (b) were imported into an automatic defect-sizing software developed in Labview. This algorithm uses a near-neighborhood-thresholding algorithm (sometimes also called as water-flow algorithm). Here, the algorithm starts from the middle of the defect and searches for the neighboring pixels if they are within the limits of a threshold set by a criterion defined by the operator. Then it proceeds to expand outwardly until no adjacent pixel satisfies the threshold criteria. The defect-sized images are illustrated in Figs. 11(a) and (b), respectively.

It can be clearly observed from Fig. 11(a) that the fiber pattern will lead to significant over-sizing of the defect when compared to the image that has been processed using DFB algorithm.

### 3.2. Segmentation of seamless tube MFL images

MFL nondestructive evaluation (NDE) of pipelines involves the analysis of huge volume of data that must be done in an automated manner to improve sensitivity (defects 5–10% of wall thickness) and decrease turn around

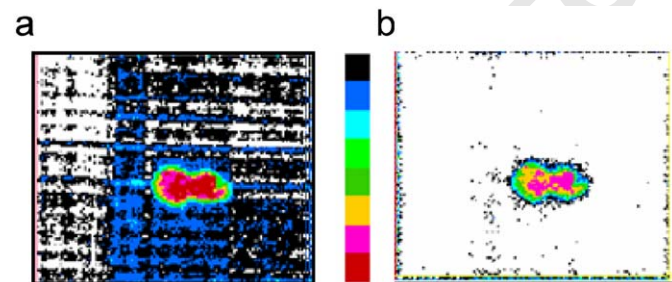


Fig. 11. Result from the automated defect-sizing software on the original C-scan image and (b) result of automated defect sizing on the DFB-processed image.

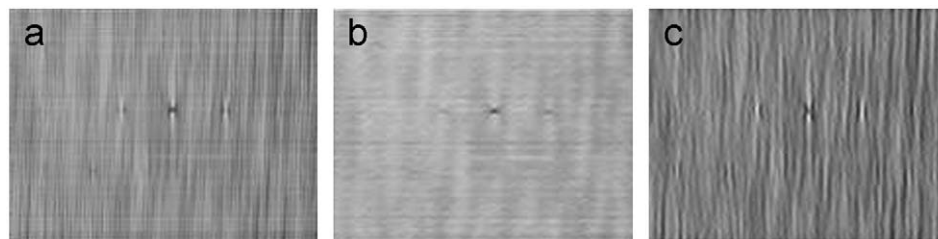


Fig. 12. (a) MFL image from a seamless pipe, (b) Image after separation of the grain noise and (c) image showing the grain pattern.

time between actual pigging and receipt of inspection results. Seamless pipes are usually produced in smaller girths (less than 24 inches); consequently, they are commonly found in the collection and distribution ends of the pipeline network. Since these types of lines are usually located close to populated areas, any failure can be potentially catastrophic. It is therefore important that any anomaly in these pipes be detected in a timely and accurately manner. The helical nature of the manufacturing operations set the grain of the seamless pipe giving rise to image artifacts known as seamless pipe noise. The MFL signal due to defects looks very similar in shape and appearance to the signals generated by grain noise and can in some cases completely mask the signals from certain type of defects.

Fig. 12(a) shows a MFL image from a seamless tube specimen with defects that were determined using MFL inspection. Previously, adaptive signal-processing techniques [9] have been used to isolate the defect features from the grain pattern. The same objective can be attained using a DFB as depicted in Fig. 12(b). The segmented image containing the grain pattern is shown in Fig. 12(c).

### 3.3. Segmentation of IR images of solar cell panels

Fig. 13(a) shows an IR image of a solar cell panel. The image also shows indications of a crack oriented at 45° to the grid lines. These cells are made from processing thin (100–200 μm) mono-crystalline Si wafers of 200–300 mm diameter that are prone to cracks. Solar cells differ from wafers in that the cells have numerous contact grid lines on both sides, while the wafers do not. These contact lines are on both sides of the cells along two orthogonal directions, and appear very prominently in the IR images. With wafers, in theory, it should be easier to identify cracks. However, in the case of the solar cells, in order to identify the cracks, it is important to find a way to subtract or ignore these contact grid lines from the IR images and highlight the cracks. An interesting artifact of these cells is that the cracks are almost always at 45° to the contact lines (by design) because of the orientation of the crystal structure of the material. Thus, this problem is an excellent case study for the use of directional filters.

Fig. 13(b) and (c) show the grid lines and the crack image, respectively, after segmentation through an 8-band DFB. Fig. 13(d) shows the crack after segmentation

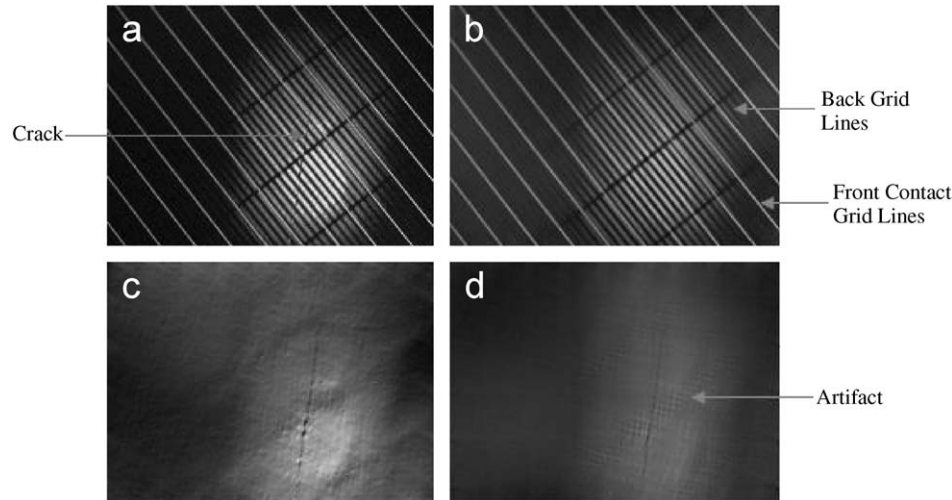


Fig. 13. (a) IR image of a solar cell with a crack, (b) Image with only the contact grid lines extracted using DFB, (c) image containing the crack extracted using the DFB and (d) image containing the crack extracted using the 2-D FFT masking algorithm.

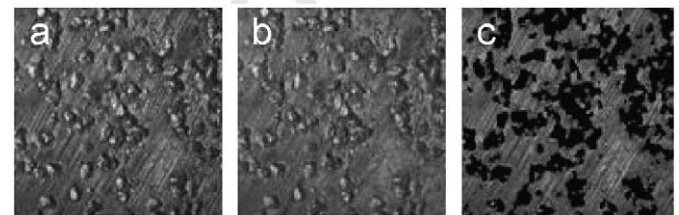


Fig. 14. (a) Image of shot-peened surface, (b) segmented image without the machining marks and (c) Image showing the segmented shot impact zones.

effectively used to segment the machining marks from the shot-peened surface information. Also since this process does not depend on the relative energy content of the image features it is not affected by the illumination conditions.

Fig. 14(a) shows the photograph of a shot-peened surface. The machining marks are clearly seen in the image. Fig. 14(b) shows the segmented image devoid of the machining marks. Fig. 14(c) shows the image in which the shot impacts have been segmented out. The above segmentation was achieved by applying an image segmentation procedure to the machine marks removed image [11].

#### 4. Conclusions

The application of the DFB towards segmentation of images from NDE inspection was demonstrated in the previous section. The DFB is a valuable tool for carrying out directional segmentation of images. The property of PR lends robustness to the segmentation, as no information is lost during the decomposition process. The use of DFB can lead to considerable simplification of image analysis tasks where complex two-dimensional textures are encountered.

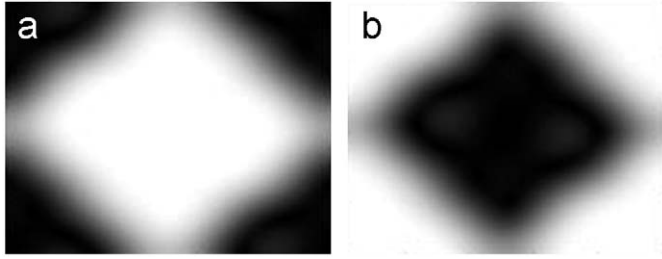


Fig. 15. (a) Frequency response of analysis filter  $H_0$  and (b) frequency response of analysis filter  $H_1$ .

The DFB has a vast potential for application in feature based image segmentation and in the automated analysis of NDE images for defect sizing and defect characterization. This may also have applications in the area of material characterization and other image-processing applications.

## Appendix A

### A.1. Design of analysis and synthesis filters

The analysis and synthesis filters form a part of the transformation chain and their design to satisfy certain key properties is discussed in this section. For obtaining a directional decomposition (wedge-shaped frequency responses for the sub-band images) the analysis filters  $H_0$ ,  $H_1$  must have frequency responses as shown in Fig. 15(a) and (b), respectively.

In addition to obtaining a directional decomposition the filter bank is designed to incorporate the property of PR or alias free reconstruction. The filter bank is said to be PR if the sum of all sub-band images is the same as the input image. It can be proved that if PR is satisfied for the two-band decomposition then the filter bank is PR for any number of cascades of the two-band decomposition. The filter bank is PR if the two sub-band outputs  $y_1$ ,  $y_2$  for the 2-band decomposition, shown in Fig. 5, satisfy the condition

$$y(n) = y_1 + y_2 = x(n). \quad (4)$$

The PR condition can be obtained in terms of the analysis and synthesis filters by expressing these filters in terms of their polyphase components. The analysis filters can be expressed in terms of their polyphase components using their Z-transforms as shown below.

$$\begin{aligned} H_0(z) &= H_{00}(z^D) + z_1^{-1} H_{01}(z^D), \\ H_1(z) &= H_{10}(z^D) + z_1^{-1} H_{11}(z^D). \end{aligned} \quad (5)$$

The above equation can be expressed as

$$\begin{bmatrix} H_0 \\ H_1 \end{bmatrix} = H_p(z^D) \begin{bmatrix} 1 \\ z_1^{-1} \end{bmatrix}, \quad (6)$$

where,  $H_p(z)$  is the polyphase matrix of the analysis filters containing the polyphase components  $H_{00}$ ,  $H_{01}$ ,  $H_{10}$ ,  $H_{11}$  of the filters  $H_0$  and  $H_1$ , respectively. More details on

polyphase decomposition can be found in [12]. The synthesis filters  $G_0$ ,  $G_1$  can similarly be expressed in terms of their polyphase components with  $G_p(z)$  being the associated polyphase matrix. Alleback and Viscito [13] showed that a 2D filter bank satisfies PR if the following condition is satisfied:

$$G_p(z)H_p(z) = I. \quad (7)$$

Eq. (7) suggests that once the analysis filters have been designed to satisfy the required pass band characteristics, the synthesis filters can be obtained by inverting the polyphase matrix of the analysis filters.

This approach poses the problem that an arbitrary  $H_p(z)$  may be difficult to invert and the synthesis filters that result will almost always be IIR. This problem can be overcome by assuming a paraunitary formulation (see [14]) for the polyphase matrix of the analysis filters as shown below.

$$\begin{aligned} H_p(z_1, z_2) &= \begin{bmatrix} \cos \theta_0 & \sin \theta_0 \\ -\sin \theta_0 & \cos \theta_0 \end{bmatrix} \prod_{i=1}^{q+r} \begin{bmatrix} z_i^{-1} & 0 \\ 0 & 1 \end{bmatrix} \\ &\times \begin{bmatrix} \cos \theta_i & \sin \theta_i \\ -\sin \theta_i & \cos \theta_i \end{bmatrix}. \end{aligned} \quad (8)$$

Here,  $q$ ,  $r$  determines the filter order in the two dimensions and  $\theta_i$ 's represent the degrees of freedom. The problem is to obtain the variables  $\theta_i$  such that the analysis filters  $H_0$ ,  $H_1$  have the required pass band characteristics. This can be solved using standard optimization techniques. Once all the variables in the polyphase matrix have been determined the analysis filters can be obtained using Eq. (5). The impulse responses of the analysis filters  $H_0$ ,  $H_1$  designed using this approach (for  $q = r = 4$ ) are given in Table 1(a) and (b), respectively. The impulse response of the synthesis filters can be obtained using the relation (3).

## References

- [1] Dudgeon DE, Mersereau RM. Multidimensional digital signal processing. Englewood Cliff, NJ: Prentice-Hall; 1984.
- [2] Mallat SG. Multifrequency channel decomposition of images and wavelet models. IEEE Trans Acoust Speech Signal Process 1989;37(12):2091–110.
- [3] Bamberger R, Smith JT. A filter bank for the directional decomposition of images: theory and design. IEEE Trans Signal Process 1992;40(4):882–93.
- [4] Liu VC, Vaidyanathan PP. Alias cancellation and distortion elimination in multi-dimensional QMF banks. IEEE Int Symp Circuits Syst 1988;2:1281–4.
- [5] Vaidyanathan PP. A tutorial on multirate digital filter banks. IEEE Int Symp Circuits Syst 1988;3:2241–8.
- [6] Sullivan R, Balasubramaniam K, Bennett A. Plate wave flow patterns for ply orientation imaging in fiber-reinforced composites. Mater Evaluat 1996;54(4):518–23.
- [7] Ji Y, Sullivan R, Balasubramaniam K. Guided wave behavior analysis in multi-layered inhomogeneous anisotropic plates. Review of progress in QNDE, vol. 15. New York: Plenum Press; 1996. p. 217–22.
- [8] Fei D, Liu Z, Hsu DK. Fiber orientation study using ultrasonic C-scan of ply interfaces. Rev Prog QNDE 2002;21:1070–107.

- 1 [9] Afzal M, Udpa S, Udpa L, Lord W. Rejection of seamless pipe noise  
in magnetic flux leakage data obtained from gas pipeline inspections.  
3 Rev Prog QNDE 2000;19:1589–96. 9
- [10] Leon PF. Determination of the coverage of shot peened surfaces. In:  
5 Fifth international conference on surface treatment. Seville Spain:  
WIT Press; 2002. 11
- [11] Swamy G, Sengupta A. Shadow estimation and growing for area  
7 coverage determination in a shot-peen inspection. In preparation. 13
- [12] Vaidyanathan PP. Multirate systems and filter banks. Englewood  
Cliff, NJ: Prentice-Hall; 1993.
- [13] Alleback JP, Viscito E. The design of multidimensional FIR perfect  
reconstruction filter banks for arbitrary sampling lattices. IEEE  
Trans Circuits Syst 1991;38(1):29–41.
- [14] Venkataraman S, Levy BC. A comparison of design methods for 2-D  
FIR orthogonal perfect reconstruction filter banks. IEEE Trans  
Circuits Syst II 1995;42(8):525–36.

UNCORRECTED PROOF